Materials Today Bio 7 (2020) 100058

Contents lists available at ScienceDirect

Materials Today Bio

journal homepage: www.journals.elsevier.com/materials-today-bio

Tissue mimetic hyaluronan bioink containing collagen fibers with controlled orientation modulating cell migration and alignment

A. Schwab [a], C. Hélary [b], R.G. Richards [a], M. Alini [a], D. Eglin [a], M. D'Este [a,*]

[a] AO Research Institute Davos, Clavadelerstrasse 8, 7270, Davos, Switzerland
[b] Sorbonne Université, UPMC Laboratoire de Chimie de La Matière Condensée de Paris (LCMCP), Paris, France

ARTICLE INFO

Keywords:
3D bioprinting
Extracellular matrix
Hyaluronic acid
Collagen hydrogel
Cell spheroid
Chondrogenesis

ABSTRACT

Biofabrication is providing scientists and clinicians the ability to produce engineered tissues with desired shapes and gradients of composition and biological cues. Typical resolutions achieved with extrusion-based bioprinting are at the macroscopic level. However, for capturing the fibrillar nature of the extracellular matrix (ECM), it is necessary to arrange ECM components at smaller scales, down to the micron and the molecular level. Herein, we introduce a bioink containing the tyramine derivative of hyaluronan (HA; henceforth known as THA) and collagen (Col) type 1. In this bioink, similar to connective tissues, Col is present in the fibrillar form, and HA functions as a viscoelastic space filler. THA was enzymatically cross-linked under mild conditions allowing simultaneous Col fibrillogenesis, thus achieving a homogeneous distribution of Col fibrils within the viscoelastic HA-based matrix. The THA-Col composite displayed synergistic properties in terms of storage modulus and shear thinning, translating into good printability. Shear-induced alignment of the Col fibrils along the printing direction was achieved and quantified via immunofluorescence and second-harmonic generation. Cell-free and cell-laden constructs were printed and characterized, analyzing the influence of the controlled microscopic anisotropy on human bone marrow–derived mesenchymal stromal cell (hMSC) migration. Anisotropic HA-Col showed cell-instructive properties modulating hMSC adhesion, morphology, and migration from micropellets stimulated by the presence and the orientation of Col fibers. Actin filament staining showed that hMSCs embedded in aligned constructs displayed increased cytoskeleton alignment along the fibril direction. Based on gene expression of cartilage/bone markers and ECM production, hMSCs embedded in the isotropic bioink displayed chondrogenic differentiation comparable with standard pellet culture by means of proteoglycan production (safranin O staining and proteoglycan quantification). The possibility of printing matrix components with control over microscopic alignment brings biofabrication one step closer to capturing the complexity of native tissues.

1. Introduction

Biofabrication aims at engineering constructs recapitulating the complexity of mammal tissues concerning cell types, chemical and biological gradients, and multiscale architecture.

In extrusion-based 3D printing (3DP), the resolution is determined by the size of the nozzle, printing speed and offset, and distance between the nozzle and printing surface, with resolution ranging from millimeters down to the micron range [1]. The physicochemical properties of the biomaterial and bioink directly influence the printing outcome and shape fidelity. The ink is most often a viscoelastic shear-thinning hydrogel (precursor) with good elasticity recovery after high shear and rapid gelation after extrusion [2–4]. In 3DP, resolution is typically referred to the macroscopic architecture of the printed construct rather than to the microscopic features within the printed filaments.

By combining different biomaterial ink compositions, gradients of material composition and cellular distribution can be produced using 3DP techniques [5–7]. Despite impressive advances in the design of bioinks and the printing of complex structures, the field still lacks reliable methods to mimic tissue architectures not only by replicating the extracellular matrix (ECM) composition but also by addressing the (macro) molecular organization within the biomaterial ink at (sub)micron-scale lengths, e.g. on fibrillar levels [8]. However, it is well known how microarchitectural features provide specific and unique properties to

* Corresponding author.
E-mail address: matteo.deste@aofoundation.org (M. D'Este).

https://doi.org/10.1016/j.mtbio.2020.100058
Received 7 April 2020; Received in revised form 21 May 2020; Accepted 22 May 2020
Available online 1 June 2020

natural tissues [9].

Collagen (Col) is the most abundant protein in the ECM, where it is found with a hierarchical fibrillar structure ranging from the triple helix at the molecular level up to fibrils and fibers at the microscopic level. Col structure, orientation, and spatial arrangement are fundamental toward mechanical stability and anisotropic properties of tissues [10]. The network architecture is also crucial to transmit forces to cells via cell-matrix interaction and contributes to the matrix biochemical environment [11,12].

To bring the 3DP technology one step closer to native tissue architectures, it is necessary to capture microstructures and nanostructures within macroscopically complex scaffold geometries [13]. Microarchitectural properties can be introduced with polymer self-assembling, a process in which macromolecules arrange into stable non-covalent structures. Col 1 [14], fibrin [11], cellulose [15], and silk fibroin [16] are the most prominent materials self-assembling into fibrous structures.

Most studies printing Col 1 biomaterial inks use soluble (acidic) and/or non-fibrillar Col 1 inks or blended neutralized Col 1 (Col 1 fractions). Printing an acidic or neutral Col 1 dispersion (20–40 mg/ml) of swollen Col fibrils with a high viscosity (>10^3 Pa·s at a shear rate of 0.11/s) requires subsequent lyophilization and chemical cross-linking for scaffold stabilization [17]. Neutralized non-fibrillar Col 1 (8 mg/ml) was held at low temperature before extrusion, and gelation was induced by printing at 37 °C [18]. In another study, neutralized Col 1 fractions were printed at high concentrations (20–40 mg/ml) and lower temperatures (4–15 °C) during extrusion printing and gelled within prewarmed media [19].

However, only few studies investigated the formation and presence of Col 1 fibers within the printed hydrogel construct and the influence on cell migration [20–22]. Moreover, cell embedding is limited in the aforementioned approaches either owing to acidic conditions or owing to postprocessing. Another drawback of printing neutralized Col 1 is the phase separation of the self-assembled fibrils from the liquid when extruded [22].

Hyaluronic acid or hyaluronan (HA) is another abundant ECM component osmotically capable of holding large amounts of water and thus functioning as a space filler for fibrillar matrix components, thus providing compressive strength through fluid retention [23]. To our knowledge, methods to control the orientation of Col 1 fibers within a viscoelastic HA-based matrix for biofabrication have not been addressed before. Col 1 has been shown to have cell-instructive properties, including inducing cell attachment by providing the cell adhesion ligand tripeptide arginine, glycine, and aspartate that promotes cell attachment and migration [24–26]. Case studies and clinical studies showed that Col 1 hydrogel provides a suitable 3D environment supporting cartilage defect repair [25,27–30]. In addition, Col 1 displays marked fibrillogenesis, thus allowing printing of the anisotropic features investigated in this article. Preliminary experiments (not shown) and literature reports pointed out the non-suitability of Col 2 for printing microscopic architecture [31–33].

The aim of this study was the development of a composite biomaterial ink consisting of the tyramine derivative of hyaluronan (THA) and Col 1 and the workflow to 3D print it, fabricating constructs with homogeneous composition and controlled Col fibril orientation at the microscopic level. In addition, the impact of microscopic anisotropy on the migration behavior of the embedded human bone marrow–derived mesenchymal stromal cell (hMSC) micropellets was analyzed by studying the direction of cell migration out of the micropellets (Fig. 1). In parallel, the chondropermissive properties of isotropic THA-Col 1 were investigated. To this aim, the THA was used to form a continuous matrix in which solubilized Col 1 was homogeneously dispersed; THA gelation and Col fibrillogenesis occurred without mutual interference. THA was additionally cross-linked with visible light for final shape fixation, thus achieving a uniform THA matrix containing Col fibrils, which were aligned via the shear forces experienced during the extrusion process. Fibril alignment and cytoskeleton orientation were quantified and compared with casted, isotropic constructs. hMSC micropellets were embedded in isotropic constructs with different compositions of THA and Col to compare their migration direction and chondrogenic differentiation.

2. Materials and methods

2.1. Tyramine derivative of hyaluronan synthesis

THA was synthesized as previously described [34]. In brief, HA (280–290 kDa, 5 mM carboxylic groups; Contipro Biotech S.R.O) was functionalized via 4-(4,6-dimethoxy-1,3,55-triazin-2-yl)-4-mehtylmorpholini 2um chloride (DMTMM, TDI) amidation with tyramine by mixing at a stoichiometric ratio of 1:1:1. Functionalization was performed for 24 h at 37 °C.

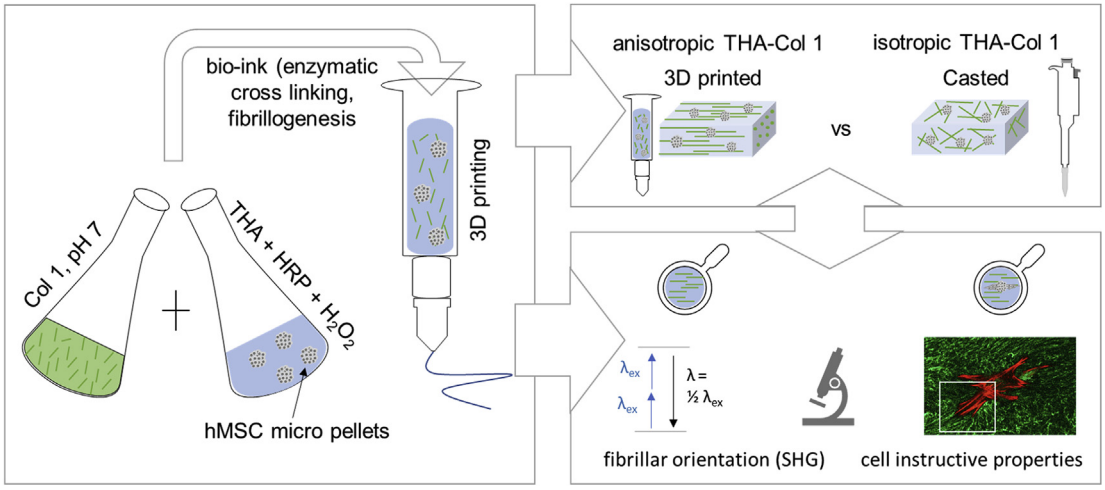

Fig. 1. Three-dimensional bioprinting as a tool to produce microscopic anisotropic scaffolds. Biomaterial and bioink were prepared by mixing neutralized Col 1 (5 mg/ml) isolated from rat tails using THA (25 mg/ml). Neutralized Col 1 was mixed with THA for enzymatic cross-linking with either cell-free or hMSC-containing micropellets. The Col 1 microstructure was investigated after 3D printing and compared with casted, isotropic samples with different microscopic techniques (second-harmonic generation [SHG] imaging and confocal microscopy). Cell-instructive properties were analyzed after *in vitro* culture on cell migration and attachment. THA = tyramine derivative of hyaluronan; Col 1 = collagen type I hydrogel; hMSC = human bone marrow–derived mesenchymal stromal cell; HRP = horseradish peroxidase; SHG = second-harmonic generation.

THA was precipitated by adding ethanol (96% v/v) dropwise, isolated using Gooch filter no. 2, and dried. The degree of substitution was 6.6% as determined by absorbance reading at 275 nm (Multiskan™ GO Microplate Spectrophotometer; Thermo Fisher Scientific).

2.2. THA-Col 1 hydrogel preparation

THA (25 mg/ml) was reconstituted with Minimum Essential Medium alpha (α-MEM; Gibco) supplemented with 10% v/v bovine fetal serum containing horseradish peroxidase (HRP; Sigma-Aldrich) at the specified concentration at 4 °C under agitation. THA for turbidity measurement was reconstituted with phosphate-buffered saline (PBS). Enzymatic cross-linking was initiated by adding different concentrations of hydrogen peroxide (H_2O_2; Sigma-Aldrich) and incubating for 30 min at 37 °C. The THA-Col 1 composite was prepared by neutralizing Col 1 (5 mg/ml, rat tail collagen I in 0.2 N acetic acid; Corning) with NaOH and adding THA before enzymatic cross-linking was initiated. Mixing ratios by volumes of THA (25 mg/ml) with Col 1 (5 mg/ml) as well as H_2O_2 concentrations are given in brackets for all experimental setups described in the following paragraphs. For cell encapsulation, hMSC micropellets were resuspended in THA before adding H_2O_2. Additional light cross-linking using 0.2 mg/ml of eosin Y as the photoinitiator (Sigma-Aldrich) was performed for all printing experiments, the corresponding control groups of casted samples, and cell migration and cell differentiation studies. Second cross-linking was needed to stabilize the (printed) structures of the enzymatically cross-linked but still soft hydrogel. Non-aligned constructs were produced by pipetting the hydrogel precursor using a positive displacement pipette (CP1000, inner diameter [ID] = 1.0 mm; Gilson) into custom-made silicon molds (6 mm in diameter). Enzymatic cross-linking was performed for all samples for 30 min at 37 °C.

To characterize the swelling and degradation of isotropic THA-Col 1, macroscopic images were analyzed by measuring the diameter of cylindrical casted hydrogels at day 0 after reaching equilibrium and after 21 days using ImageJ (National Institutes of health [NIH]).

2.3. Three-dimensional bioprinting of THA-Col

An extrusion-based bioprinter (3D Discovery™; RegenHU) was used to prepare THA-Col 1 (25 mg/ml of THA, 0.3 U/ml of HRP, 0.392 mM H_2O_2, 5.0 mg/ml of Col 1) anisotropic hydrogels (0.25″ cylindrical needles, 15G: ID = 1.36 mm, 0.2 bar, writing speed = 8 mm/s; 18G: ID = 0.84 mm, 1.6 bar, writing speed = 8 mm/s; Nordson EFD) with subsequent light cross-linking (515-nm light-emitting diode, speed = 4 mm/s). Biomaterial and bioink were transferred into 3CC barred (ID = 2.3 mm; Nordson) for enzymatic cross-linking (30 min, 37 °C), printed with the aforementioned parameters (room temperature of 20–22 °C) and transferred into culture media (cell-embedded hydrogel) or PBS (cell-free).

A complex microstructure to mimic microarchitecture of Col fibers in articular cartilage was accomplished with CAD Software (RegenHU). The fibrillar structure in the superficial zone (SZ; at the surface) was realized by printing 3 layers of parallel lines, whereas the middle zone (MZ) and deep zone (DZ) were designed as circular structures to mimic the arch-like geometry.

2.4. Rheological characterization

Viscoelastic properties of the biomaterial inks were analyzed using the Anton-Paar MCR-302 rheometer with 1° cone-plate geometry and a gap distance of 0.049 mm at 20 °C. Silicone oil (Sigma-Aldrich) was applied to the external border to prevent drying during the measurement. Viscosity was measured with a shear rate ranging from 0.011/s to 1001/s (n = 2/group) to evaluate shear thinning behavior of the enzymatically cross-linked THA (0.3 U/ml of HRP, 0.52 mM H_2O_2), THA-Col 1 (1:1 v/v), and Col 1 in a rotational experiment.

Oscillatory tests (amplitude sweep: frequency = 1 Hz, amplitude = 0.01–100% strain; frequency sweep: amplitude = 1% strain, frequency = 0.01–100 Hz, n = 2/group) were performed using the parallel-plate measuring system at 20 °C to characterize the elastic modulus of THA and THA-Col 1 at varying polymer concentrations (0.3 U/ml of HRP, 0.65 mM H_2O_2).

2.5. Turbidity measurement

Fibrillation of Col 1 was evaluated by the absorbance reading at 313 nm at 37 °C at 5, 30, and 60 min after induction of neutralization of Col 1 and enzymatic gelation (n = 2–5 samples/group) of THA using a Multiskan™ GO Microplate Spectrometer (Thermo Scientific). When Col 1 starts to fibrillate, the solution turns from transparent to opaque (more turbid), which is associated with an increase in optical density [35–38]. The following solutions were analyzed: neutralized Col 1, acidic Col 1, THA (0.075 U/ml of HRP, 0.26 mM H_2O_2), and THA-Col 1 (1:1 and 1:2 v/v) composite undergoing enzymatic cross-linking during measurement of Col 1 fibrillogenesis. Temperature was held at 37 °C to induce enzymatic cross-linking of THA and stabilize Col 1 fibrillation.

2.6. Second-harmonic generation imaging

To visualize Col 1 fibers (0.3 U/ml of HRP, 0.52 mM H_2O_2) (1:1 v/v), second-harmonic generation (SHG) images were acquired using the MaiTai multiphoton laser–equipped confocal microscope (Leica SP8). The SHG signal was collected using a HyD detector between 437 and 453 nm (λ_{ex} = 880 nm, output power ap 1.7 W). In addition, the transmitted light and autofluorescence signal (510–600 nm) was acquired at varying emission wavelength for the SHG detector (λ_{em} = 420–436 nm and λ_{em} = 454–470 nm) to check for the specificity of the SHG signal at 437–453 nm. For deep imaging, a long-distance objective (25× water immersion objective) was used to acquire z-stacks with optimal settings for each sample. Image series acquired using Leica Application Suite X software (LAS X; Leica) were processed using ImageJ (NIH).

2.7. Cell culture

2.7.1. Cell isolation

hMSCs were isolated from the bone marrow aspirate with full ethical approval (Ethics Committee of University of Freiburg Medical Centre-EK-Freiburg: 135/14), as described in a previous study [39]. hMSCs were subcultured on α-MEM (Gibco) supplemented with 10% v/v Sera Plus bovine serum (PAN Biotech), 100 U/ml of penicillin, 100 μg/ml of streptomycin (Gibco), and 5 ng/ml of basic fibroblast growth factor (Fitzgerald Industries International) in a humidified atmosphere of 5% CO_2, with the medium being changed every second day.

2.7.2. Three-dimensional cell migration and viability study

To analyze directed cell migration within a 3D environment, cell micropellets, also known as cell aggregates, were embedded in different hydrogels. Cell spheroids were prepared from hMSCs (passage 3–4) in an ultralow attachment Petri dish (Corning) with α-MEM media supplemented with 10% bovine serum, 100 U/ml of penicillin, and 100 μg/ml of streptomycin via self-assembly to form cell aggregates. After 3 days, the cell aggregates were harvested, centrifuged (5 min, 500 g), and suspended in a minimum volume of culture media to mix with the hydrogel precursor solution before initiating (enzymatic) cross-linking for THA-Col 1 (1:1 v/v) or THA (0.3 U/ml of HRP, 0.39 mM H_2O_2) or neutralizing Col 1 at a final cell density of 3 Mio/ml and cultured for 8 days. For THA-Col 1 and THA, an additional light cross-linking of printed and casted samples was carried out at 515 nm.

To evaluate cell migration, samples harvested at day 0, 3, and 8 were stained with phalloidin as described in Section 2.8.1, and fluorescent images were taken for subsequent quantification of migration length and area (n = 3–5 micropellets/time point) described in Section 2.9. In

addition, embedding of cell micropellets allowed analysis of the direction of cell migration.

Live and dead assay was performed during the migration experiment of hMSC micropellets embedded in THA-Col 1 (0.3 U/ml of HRP, 0.39 mM H_2O_2, 1:1 v/v) of 3D printed and casted samples at day 1 and day 6. H_2O_2 concentration was selected in a range that is known not to be toxic to cells [40]. After washing with PBS, the samples were incubated with 2 μM calcein AM (Sigma-Aldrich) and 1 μM ethidium homodimer-1 (Sigma-Aldrich) for 30 min at 37 °C, washed with PBS, and imaged using a confocal microscope (LSM800; Carl Zeiss). Dead cells were stained in red with ethidium homodimer-1 (λ_{ex} = 561 nm), and the cytoplasm of living cells was stained in green with calcein AM (λ_{ex} = 488 nm).

2.7.3. Chondrogenic differentiation

For chondrogenic differentiation, hMSCs (passage 2) were seeded in a 6-well microwell plate (AggreWellTM 400 plate) at 1.67 Mio/well according to the manufacturer's protocol and cultured for 3 days to form cell micropellets. Chondrogenic media was composed of high-glucose Dulbecco's Modified Eagle Medium (Gibco) supplemented with non-essential amino acids (1% v/v; Gibco), ascorbic acid 2-phosphate (50 μg/ml; Sigma-Aldrich), dexamethasone (100 nM; Sigma-Aldrich), ITS + premix (1% v/v; Corning), transforming growth factor beta (TGF β1, 10 ng/ml; Fitzgerald), and antibiotics (100 U/ml of penicillin, 100 μg/ml of streptomycin; Gibco). The cell micropellets were embedded in THA-Col 1 (0.5 U/ml of HRP, 0.65 mM H_2O_2, 5% w/v Col 1, 1:1 v/v) at a final cell concentration of 5 Mio/ml hydrogel volume (400,000 cells/scaffold) before enzymatic gelation, additionally light cross-linked, and cultured for 21 days in chondrogenic media. The medium was changed 3 times a week. For the positive control, standard hMSC pellets were prepared by seeding 250,000 hMSCs into each V-bottom 96-well plate (Ratiolab) and culturing under the same conditions.

2.8. Histological processing and staining

2.8.1. Actin filament-Col 1 immunofluorescence staining

For actin filament staining in combination with Col 1 immunofluorescent staining, printed and casted THA-Col 1 (1:1 v/v) was fixed with 4% neutral buffered formalin (Formafix AG) at room temperature and stored in PBS at 4 °C upon staining.

Cytoskeletal organization of hMSC migration from cell micropellets embedded in enzymatically cross-linked THA-Col 1 samples (0.3 U/ml of HRP, 0.39 mM H_2O_2) was analyzed on day 0 and after 6 days of culture, with phalloidin staining to visualize actin filaments. Hydrogels were permeabilized with 0.5% v/v Triton X-100 (Sigma-Aldrich) for 10 min at room temperature, blocked with 10% bovine serum (Sera plus) for 30 min, and stained with phalloidin-TRITC (2 μg/ml, P1951; Sigma-Aldrich) for 45 min at room temperature. Immunofluorescence staining for Col 1 was processed directly after phalloidin staining by overnight incubation with the primary antibody (COL 1, 1:5,000 dilution with PBST, monoclonal; Sigma-Aldrich). The secondary antibody goat anti-mouse, Alexa fluor 488 (1:600 diluted with PBST; Invitrogen) was incubated for 1 h. Cell nuclei were stained with 4′,6-diamidino-2-phenylindole (DAPI, 2 μg/ml; Sigma-Aldrich) for 10 min. The samples were washed between every step with Tween-20 (0.1% v/v, P1379; Sigma-Aldrich) in PBS and stored in PBS for microscopy.

A confocal microscope (LSM800, Carl Zeiss) was used to acquire fluorescence images (25× and 40× water immersion objectives) to visualize Col 1 matrix and cells. Col 1 fibers within the hydrogel matrix were stained in green (λ_{ex} = 488 nm), the cell cytoskeleton was stained in red (λ_{ex} = 561 nm), and cell nuclei were stained in blue with DAPI (4′,6-Diamidin-2-phenylindol) (λ_{ex} = 405 nm). For all samples, z-stack images were acquired for the three single channels and processed using ImageJ (NIH) to generate 2D z-projection (maximum intensity) images. Brightness and contrast settings were adjusted to increase contrast of the single-channel images. Merged images of single channels were created using the image overlay tool (merge channels) of ImageJ software (NIH). Images of Col 1–stained samples and the cytoskeleton were further processed using ImageJ to quantify fiber orientation and direction of migration, as described in Section 2.10.

2.8.2. Cryoembedding

For histological staining, the samples were fixed for 30 min with 4% neutral buffered formalin (Formafix AG) at room temperature and stored, washed with PBS, and processed with sucrose (150 mg/ml and 300 mg/ml; Sigma-Aldrich) before being embedded in tissue freezing medium (Leica). The samples were cut using a cryostat microtome (HM 500 OM; Zeiss) to 8-μm slices and kept at −20 °C until they were being processed for histological staining with safranin O-fast green.

2.8.3. Safranin O-fast green staining

To stain the proteoglycans in the ECM within the hydrogel samples and cell pellets, safranin O staining was performed after 21 days of chondrogenic differentiation. The slides were washed with water to remove the cryocompound and stained with Weigert's hematoxylin (12 min, room temperature; Sigma-Aldrich), blued with tap water (10 min), rinsed with deionized water, and stained with fast green (0.02% w/v; Fluka) for 6 min to visualize collagenous matrix in green/blue. After washing with acetic acid (1%; Fluka), the samples were incubated with safranin O (0.1%, 15 min; Polysciences) to stain proteoglycans in red. After washing with deionized water, staining was differentiated with ethanol (70%; Alcosuisse) and subsequently dehydrated with series of alcohols (96% ethanol, ethanol absolute, xylene) and sealed using a coverslip (Eukitt; Sigma-Aldrich). Microscopic evaluation was performed using a bright-field microscope (Olympus BX63; Olympus).

2.9. Quantification of cell migration length and area

A sprout morphology tool in ImageJ (NIH) was used to quantify the migration length on phalloidin-stained MAX projection images. For bead and sprout detection, the mean threshold method was selected with sample-specific adjustment of values (bead detection: blur radius for bead detection = 1.0, minimum bead radius = 30–110 μm, dilate beads by factor 1.0–2.8; sprout detection: sprout detection radius = 1.0 μm, minimal plexus area = 5,000 μm^2, minimal sprout area = 500 μm^2). Migration area was calculated based on the resulting black-and-white mask from the sprout morphology tool results with region of interest (ROI) area measurement. The calculated area includes the area of the cell micropellets.

2.10. Evaluation of Col 1 fiber and cytoskeleton alignment

Two-dimensional fast fourier transform (FFT) of images acquired with SHG and confocal microscopy for Col 1 immunostaining were used for the evaluation of Col 1 fiber alignment. For both microscopic techniques, single-channel images at one focus plane were used (n = 2–3 samples with 3 focus planes at the beginning, center, and end of a printed filament) to investigate the homogeneity of alignment at different z-locations within the strut. For quantification of cytoskeleton orientation, MAX projection images of the red channel (561 nm) of 4 micropellets at day 6 were processed. The Oval profile plug-in in ImageJ (NIH) was chosen for quantitative evaluation of the Col 1 fiber and cytoskeleton orientation, as described in detail in the studies of Tognato et al. [41] and Ayres et al. [42]. In brief, single fluorescent or SHG images were processed using ImageJ (NIH) as follows: Select Process-Filters to unsharp mask, then go to Process- FFT for FFT transformation of the image, continue selcting Image - Transform to rotate 90 °C right, and then select Process - FFT to, make a circular selection with radius 512. Finally choose Oval Profile under Plugins for performing Circumferential profile with analysis mode radial sum and number of points 360. The resulting gray values were normalized to the maximum gray values of each single image, and mean values including standard deviation for both SHG and confocal images are shown in the bar diagram.

2.11. Gene expression analysis: real-time quantitative polymerase chain reaction

Total RNA was isolated from the samples (THA-Col 1, THA-Col 1 MSC, and MSC pellet) at day 0, 14, and 21 using TriReagent® (Molecular Research Center Inc.) following the manufacturer's protocol. RNA quantity was measured using the NanoDrop 1000 spectrophotometer (Thermo Fischer). cDNA synthesis of 1 μg of RNA was performed using Vilo Superscript (Invitrogen) according to the manufacturer's protocol. Reverse transcription was carried out using Thermocycler (Mastercycler gradient; Eppendorf) including preheating at 25 °C for 10 min, followed by 42 °C for 120 min, inactivation of reverse transcriptase for 5 min at 85 °C, and cooling down to 4 °C.

For real-time polymerase chain reaction (PCR), 10 μl of the reaction mixture containing TaqMan Universal Master Mix (Thermo Fischer), the primer and probes, diethylpyrocarbonate (DEPC) water, and cDNA was loaded into 384 well plates. PCR was run with an initial heating to 50 °C for 2 min, followed by heating at 95 °C for 10 min and 40 cycles at 95 °C for 15 s with annealing at 60 °C for 1 min.

Relative gene expression of the chondrogenesis-associated genes aggrecan (*ACAN*), Col type 2 (*COL2A1*) and *SOX9*, fibrous- and hypertrophy-associated genes Col type 1 and type X (*COL1A1*, *COL10A1*), *RUNX2*, and the endogenous control ubiquitin C (*UBC*) was calculated using $2^{-\Delta\Delta Cq}$. The *UBC* housekeeping gene has been proven to be stable in the present conditions. Two different controls MSC pellets and MSCs embedded in THA-Col 1 at day 0 were used for the respective samples. Details on the primers and probe sequence as well as catalog numbers of Assay-on-Demand (Applied Biosystems) are listed in Supplementary Material (Table A1).

2.12. Quantification of glycosaminoglycans and DNA

To quantify glycosaminoglycans (GAGs) and DNA within MSC pellets and cell-free and cell-laden THA-Col 1 hydrogels (n = 3 samples/group and time point), the samples were digested with proteinase K (0.5 mg/ml; Sigma-Aldrich) at 56 °C. DNA content was measured in duplicate using the Quant-iT™ PicoGreen (Invitrogen) assay according to the manufacturer's instructions. Fluorescence was measured using a plate reader (Tecan infinite 200 PRO; Tecan) at 485-nm excitation wavelength and 535-nm emission wavelength including a DNA standard curve. The amount of proteoglycans was determined in duplicate using the dimethylene blue dye method with absorbance measurement at 535 nm including a chondroitin 4-sulfate sodium salt from the bovine trachea (Fluka BioChemika) standard [43]. For calculation of GAGs released into media, the values of cell-free THA-Col 1 were subtracted from the results of hMSCs embedded in THA-Col 1.

2.13. Statistical analysis

All samples were measured in technical duplicate of 2–4 biological replicates per group and time point and displayed as a box plot including the mean value or as mean values with standard deviation. Statistical analysis was performed using GraphPad Prism (Prism 8, USA). Cell migration length and migration area as well as PCR data was analyzed using the multiple *t*-test. Values of the three sample groups (THA, Col 1, and THA-Col 1) were compared at three time points (day 0, day 3, and day 8) and corrected for multiple comparisons using the Holm-Sidak method. Normalization of GAG-to-DNA values was performed using two-way analysis of variance (comparing means of each sample between day 0 and day 21 and between samples at the two time points) with the Sidak post hoc test to correct for multiple comparisons. Statistical significance was assumed for *p*-values <0.05.

3. Results

3.1. Morphology and mechanical properties of the composite network

THA-Col 1 composites were prepared dispersing Col 1 into THA, with fibrillogenesis induced by the pH rise and THA cross-linking triggered by H_2O_2 addition and incubation at 37 °C. The presence of Col 1 fibers in

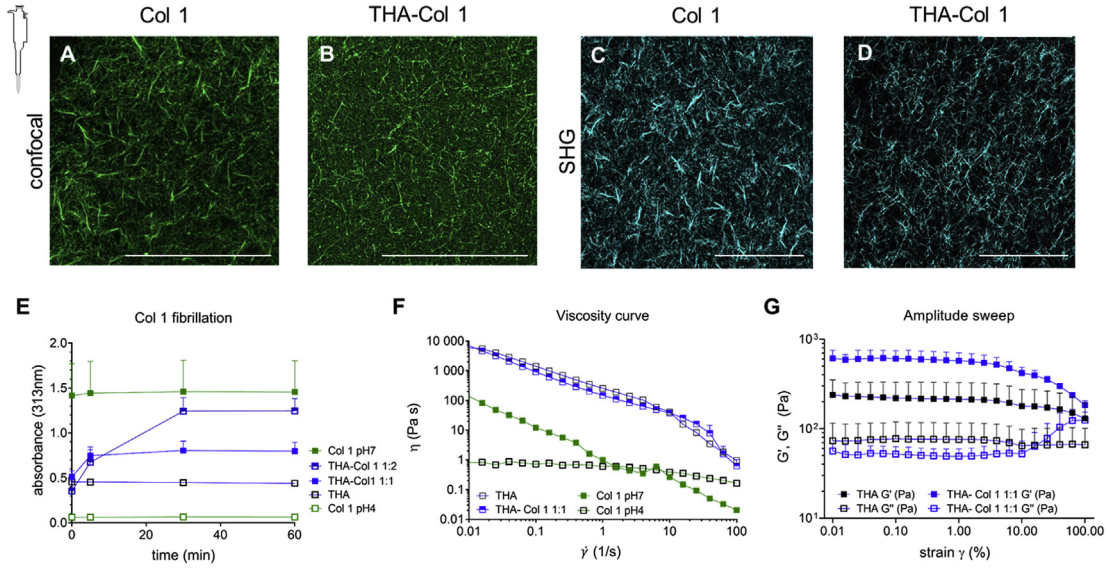

Fig. 2. Collagen (Col 1) fibril distribution in THA hydrogel and rheological properties. (A) Visualization of Col 1 fibrils within Col 1 hydrogel and (B) THA-Col 1 hydrogels using confocal imaging (immunofluorescent staining for Col 1) and (C–D) SHG imaging (no labeling), respectively. Both techniques illustrate homogenous distribution of Col 1 fibrils (scale bar = 100 μm). (E) Turbidity measurement of THA-Col 1 demonstrated Col 1 fibril formation in the composite dependent on Col 1 content. The more the presence of Col 1 in the composite, the higher the absorbance at 313 nm over time, with maximum values for Col 1 only. (F) Viscosity curve (as function of the shear rate) demonstrates shear thinning behavior of THA, THA-Col 1, and neutralized Col 1, marked by decreasing viscosity with increasing shear rate. Col 1 (pH 7, 5 mg/ml) showed lower viscosity than THA (25 mg/ml) and THA-Col 1. Acidic Col 1(pH 4, 5 mg/ml) lacks shear thinning behavior with a constant viscosity over a range of tested shear rates. (G) Rheological characterization (amplitude sweep, 1 Hz) to evaluate mechanical properties of biomaterial ink by means of storage (G') and loss (G") modulus of THA-Col 1 and THA after enzymatic cross-linking. Storage modulus increases in the composite compared with THA. THA = tyramine derivative of hyaluronan; SHG = second-harmonic generation; Col 1 = collagen type I hydrogel.

THA-Col 1 composite hydrogels was characterized by three independent techniques: SHG imaging, confocal microscopy, and turbidimetry (Fig. 2). As the positive control, Col 1 hydrogel was included for all measurements. The turbidity measurement allowed evaluation of the fibrillogenesis kinetics (Fig. 2E). An increase in absorbance (313 nm) over time was observed to be ranging from 0.4 to 0.8 for THA-Col 1 (1:1) and from 0.06 to 1.3 for THA-Col 1 (1:2), indicative of Col 1 fibrillation within the composite. The maximum absorbance values increased with the Col 1 content within the materials, with the highest values around 1.5 absorbance units for the neutralized Col 1 positive control, which was fibrillar from the beginning of the measurement. After 30 min of incubation at 37 °C, a plateau was reached for all groups. Pure Col 1 in acidic and in neutralized solution, and THA showed constant values in turbidity assay without change in absorbance values over time.

The fibrillation of Col 1 was further corroborated by imaging techniques. Both SHG imaging (Fig. 2C and D) and confocal microscopy of Col 1 immunofluorescent stained samples (Fig. 2A and B) showed the obvious presence of Col 1 fibers with a homogenous distribution within THA. Fiber morphology was visibly different, with a thinner and a denser fiber network in THA-Col 1 than in the Col 1 control. Quantification of fibril size and distribution was not possible because the fibrils cross different focal planes resulting in non-reliable values. Images acquired by confocal and SHG microscopy illustrate an identical trend in fibrillar characteristics.

HRP concentration, H_2O_2 content, and mixing ratios of THA and Col 1 were selected based on the requirements for rheological properties and extrudability of the biomaterial ink and Col 1 fibrillogenesis. The viscosity curve clearly demonstrated the shear thinning behavior of the biomaterial ink, with an overall higher viscosity of 7 kPa s for THA-Col 1 and 6 kPa s for THA at 0.011/s and monotonic decrease for increasing shear rates. At a shear rate higher than 50/s, the viscosity of THA-Col 1 fell below the value for THA. Neutralized Col 1 (5 mg/ml) viscosity was overall lower, ranging from 0.13 k Pa·s at 0.011/s to 1 Pa s at 11/s. Acidic Col 1 (pH = 4) showed an evident reduction in shear thinning, with viscosity ranging from 0.8 Pa s to 0.6 Pa s. Therefore, THA-Col 1 retained the shear thinning behavior required for the biomaterial ink extrusion. An increase in storage modulus was observed in the THA-Col 1 composite hydrogel compared with THA (both samples were prepared at the same THA concentration for matching the concentrations of the enzymatic cross-linking agents, Fig. 2G).

The amplitude sweep showed a similar profile for THA and THA-Col 1, with the Col 1 presence implicating an increase in storage modulus from 220 Pa to 608 Pa at 0.1% strain, but a similar decreasing trend at higher strain (Fig. 2G). This behavior is indicative that THA viscoelastic properties are not disrupted by the formation of the composite with Col 1. Enzymatically and light cross-linked THA-Col 1 (isotropic samples) showed swelling of 150% relative to the original diameter to 0.89 ± 0.04 cm. No degradation in terms of change in sample diameter occurred in the cell-free group during incubation in media at 37 °C (0.93 ± 0.04 cm).

3.2. Cell-instructive properties of THA-Col 1 bioink

hMSCs micropellets were embedded in the bioink made of THA-Col 1 and in its single components to determine how the composition influences cell attachment and migration from the micropellets. Fig. 3A illustrates a panel of MAX projection images stained for actin filaments on day 0, day 3, and day 8. Cells migrated out of the uniformly dispersed

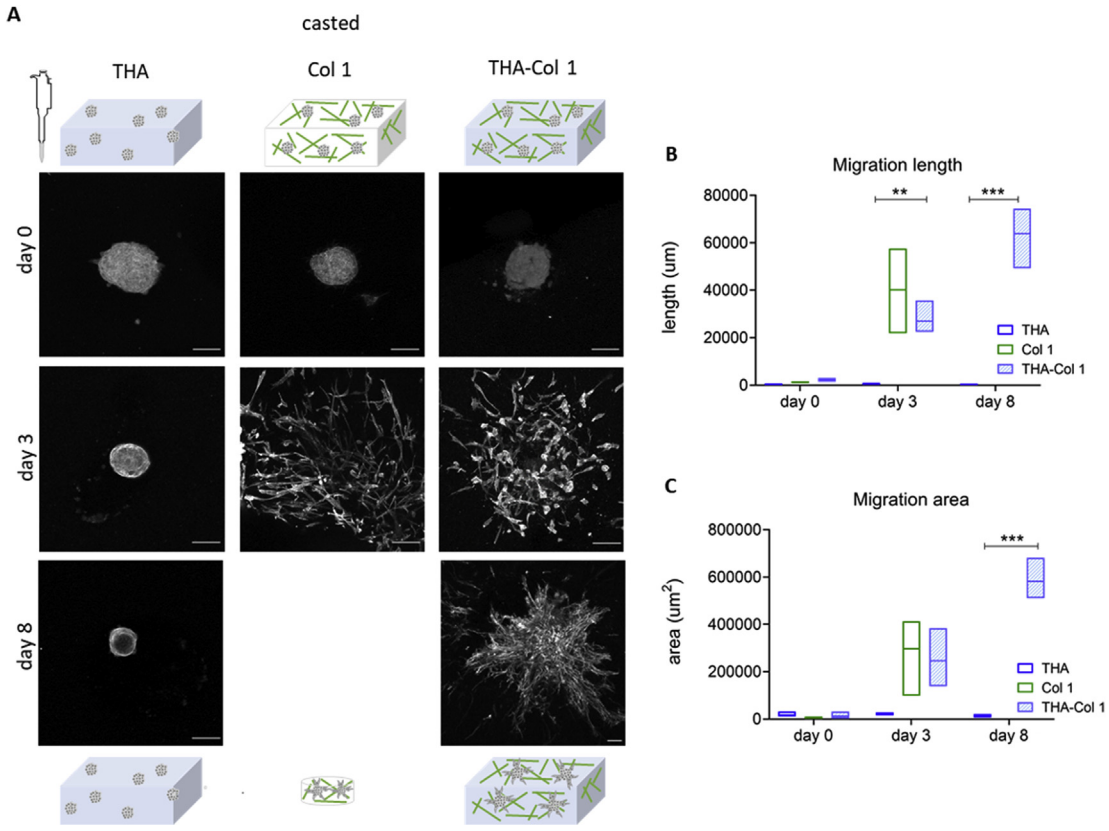

Fig. 3. Cell-instructive properties of THA-Col 1 addressing hMSC migration and cell attachment. (A) Confocal images of actin filament–stained hMSC micropellets embedded in THA-Col 1 (THA-Col 1, 25 mg/ml (1:1); Col 1, 5 mg/ml), THA (25 mg/ml), and Col 1 (5 mg/ml) at day 0, at day 3, and after 8 days of culture. Migration of hMSCs was seen in THA-Col 1 and Col 1 but not in THA. Col 1 hydrogel was shrinking over time and formed a small pellet of less than 2 mm in diameter (scale bar = 100 μm). (B) Area of cell migration and (C) migration length was higher in Col 1 than in THA-Col 1, increasing over time. Quantification of migration area and migration length. $^{**}p < 0.01$, $^{***}p < 0.001$. hMSC = human bone marrow–derived mesenchymal stromal cell; THA = tyramine derivative of hyaluronan.

micropellets into the biomaterials in the presence of Col 1 (THA-Col 1 and Col 1), whereas no migration was observed in THA hydrogels.

Migration length and migration area were quantified using the ImageJ sprout morphology tool on MAX projections images stained with phalloidin. Mean values for both parameters confirm the highest migration in Col 1 (migration length: 40,165 μm; migration area: 297 μm^2), followed by THA-Col 1 (migration length: 270 μm, $p = 0.0050$ compared with THA day 3; migration area: 246 μm^2, $p = 0.0720$ compared with THA day 3) on day 3. From day 3 to day 8, the migration increased further for Col 1 and THA-Col 1 (THA-Col 1 migration length: 638 μm, $p = 0.0005$ compared with THA day 8; migration area: 582 μm^2, $p = 0.0001$ compared with THA day 8). In THA, migration area and migration length of hMSC micropellets remained unvaried for the whole duration of the experiment. Owing to significant shrinkage of Col 1 hydrogels, the quantification of the two parameters on day 8 was not possible for Col 1 (Fig. 3B–C). The differences in spheroid size were derived from the variation in focus plane within the 3D constructs.

3.3. In vitro chondrogenic differentiation

Chondrogenic differentiation potential of hMSC micropellets embedded in isotropic THA-Col 1 was compared with hMSC pellet culture as the positive control and was evaluated by qPCR, safranin O staining, and total GAG/DNA content analysis. Gene expression analysis of hMSC spheroids embedded in THA-Col 1 (Fig. 4A) showed an increase in chondrogenesis-related markers *COL2A1* (1,000–10,000 fold), *ACAN* (10–1,000 fold), and *SOX9* (<20 fold) over time, similar to hMSC pellets. *COL1A1* was slightly downregulated (0.1–1.0 fold), whereas *COL10A1* showed an increase of up to 100-fold for the two groups at day 14. At day 21, *COL10A1* stayed constant for hMSC-embedded THA-Col 1, whereas the fold change relative to the control sample decreased to <10 for hMSC pellets. *RUNX2* upregulation was much less pronounced (<10-fold change) than the expression of ECM-associated genes. The ratio of *COL2A1/COL1A1* (Fig. 4B) was higher for hMSC micropellets embedded in THA-Col 1 (day 14: 5353 ± 1699, $p = 0.0242$ compared with day 0, day 21: 1650 ± 409, $p = 0.0293$ compared with day 0) than for hMSC pellets (day 14: 931 ± 568 $p = 0.1467$ compared with day 0, day 21: 300 ± 69 $p = 0.0260$ compared with day 0).

At day 21, an increase in proteoglycan content was observed in both groups (Fig. 4C–D). The total amount of GAGs increased from 0.46 ± 0.38 μg/ml to 4.48 ± 0.13 μg/ml ($p < 0.0001$) for hMSC pellets and from 1.18 ± 0.20 μg/ml to 4.48 ± 0.69 μg/ml ($p < 0.0001$) for hMSC micropellets embedded in the bioink. Release of proteoglycans in the media was 5.88 ± 0.92 μg and 13.58 ± 2.93 μg, respectively. Both

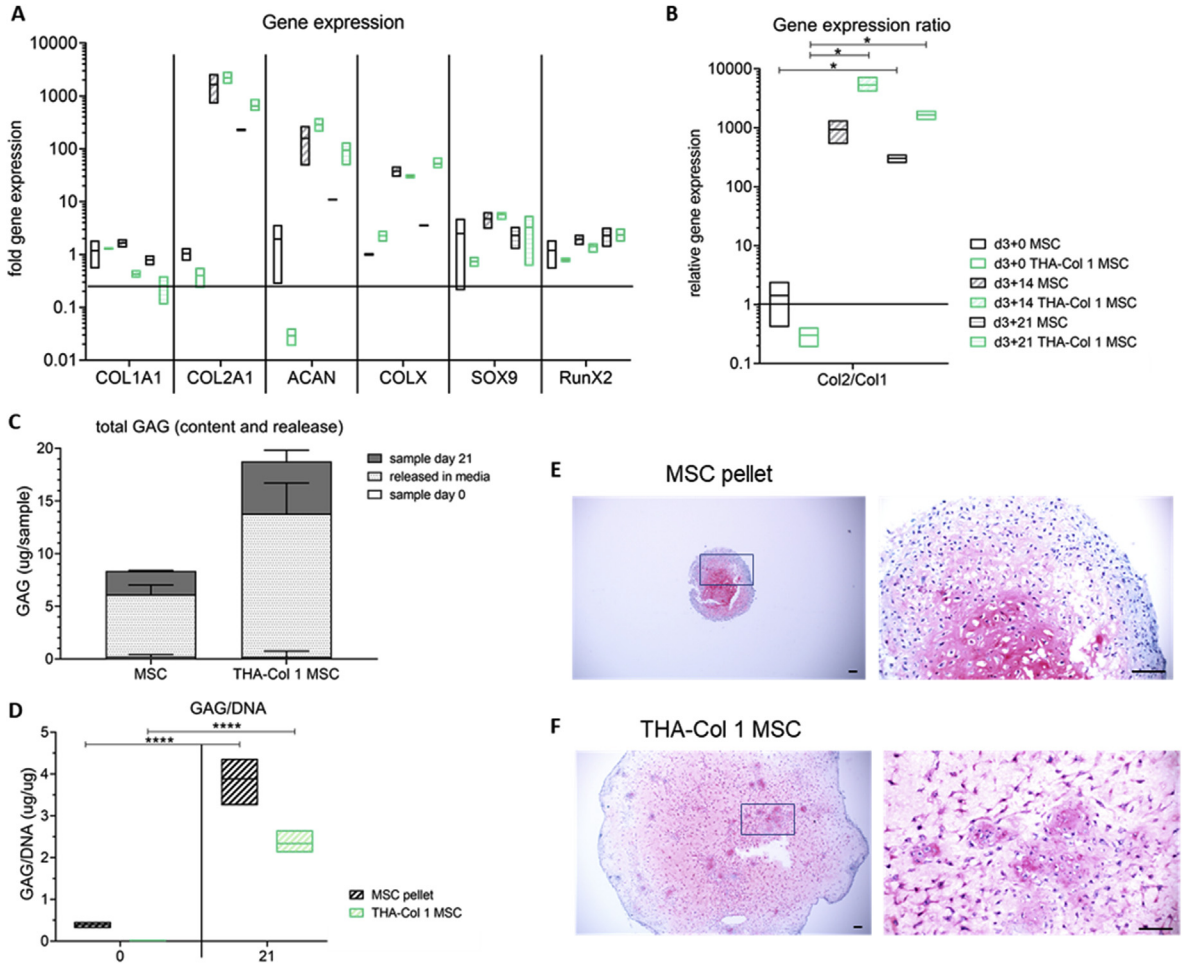

Fig. 4. Chondrogenic differentiation potential of hMSCs embedded in THA-Col 1 compared with hMSC pellet culture. (A) Gene expression analysis relative to hMSC pellets or hMSCs embedded in THA-Col 1 hydrogel (TC MSC) control at day 0 for Col 1 (COL 1A1), Col II (COL 2A1), aggrecan (ACAN), SOX9, and RunX2. Increase in expression was observed for all chondrogenesis-related genes with minor changes for SOX9 and RunnX2. (B) Relative gene expression ratio of Col 2 to Col 1 at day 21. *$p < 0.05$. (C) Quantification of proteoglycans (GAG/sample) including total amount of GAGs released into the media supernatant and GAGs retained in the sample at day 21. (D) GAG/DNA increased over time from day 0 to day 21 for MSC pellet and THA-Col 1 MSCs. ****$p < 0.0001$. (E) Safranin O staining to visualize proteoglycans in the ECM after 21 days of *in vitro* culturing at two magnifications for MSC pellets and (F) MSCs embedded in the THA-Col 1 hydrogel (THA-Col 1 MSC) (scale bar = 100 μm). PCR = polymerase chain reaction; GAG = glycosaminoglycan; THA = tyramine derivative of hyaluronan; ECM = extracellular matrix; hMSC = human bone marrow–derived mesenchymal stromal cell.

groups retained around 25% of the total produced proteoglycans within the sample (MSC pellet = 26.8%, THA-Col 1 MSC = 23.3%). Normalizing total GAG-to-DNA values in the samples increased for hMSC pellets within 21 days to 3.88 ± 0.42 ($p < 0.0001$) and for hMSCs embedded in THA-Col 1 to 2.34 ± 0.24 ($p < 0.0001$).

The histological staining confirmed the chondrogenic differentiation. After 21 days of culture, a homogenous distribution of safranin O–positive staining was observed for hMSC pellets and hMSCs embedded in THA-Col 1 (Fig. 4E–F). The hMSC micropellets were no longer visible in the point of initial seeding because of the migration throughout the whole hydrogel, resulting in a homogenous cell distribution. hMSC morphology was comparable between the cells in the pellet and the cells embedded in the hydrogel; most cells appeared to be condensed or rounded with a low population of spindle-shaped cells at day 21.

Overall, this experiment pointed out that hMSCs embedded in the isotropic THA-Col 1 bioink is permissive to cell migration and GAG retention and that it retains the same chondrogenic potential as the gold standard pellet culture.

3.4. Three-dimensional printing to fabricate microscopically anisotropic scaffolds

The enzymatic cross-linking of the THA-Col 1 biomaterial ink was optimized in terms of HRP and H_2O_2 concentrations for extrusion printing to meet the requirements of a shear thinning behavior and to be extruded as a homogenous and continuous filament. A printing speed of 8 mm/s and 4 mm/s was found to be optimal for the composite ink for the 15G and 22G needle, respectively. After optimizing THA-Col 1 biomaterial ink, the presence of Col 1 and fibrillar orientation were characterized. SHG imaging and confocal microscopy were used to visualize the Col 1 fibrils in the THA-Col 1 biomaterial ink after extrusion printing. The fibrillar structure of Col 1 in the composite was preserved after printing and resulted in an anisotropic material. Representative microscopic images in Fig. 5A and C clearly demonstrate the presence of parallel-aligned Col 1 fibers along the direction of the printing.

To further characterize this property, the ImageJ Oval plug-in was used to quantify the alignment of THA-Col 1 after printing and compare with casted THA-Col 1 and casted Col 1. Casted THA-Col 1 resulted in the least anisotropic properties, followed by casted Col 1. Comparing the peak width of the preferred orientation in the printed samples at a normalized gray value of 0.5 (SHG: 43°, confocal microscopy: 60°) with the corresponding casted one (SHG: 115°, confocal microscopy: 150°) and the casted Col 1 (SHG: 62°, confocal microscopy: 129°), a clear narrowing of the Col 1 fiber orientation dispersity was observed for the printed sample (Fig. 5B and D).

The control over the parallel fiber orientation was used to produce a construct imitating the Col orientation in knee articular cartilage. The fibrillar structure in the SZ (at the surface) was realized by printing parallel lines, whereas the MZ and DZ were realized by printing an arch-like geometry, as shown in Fig. 5E and G, with an overall sample size of

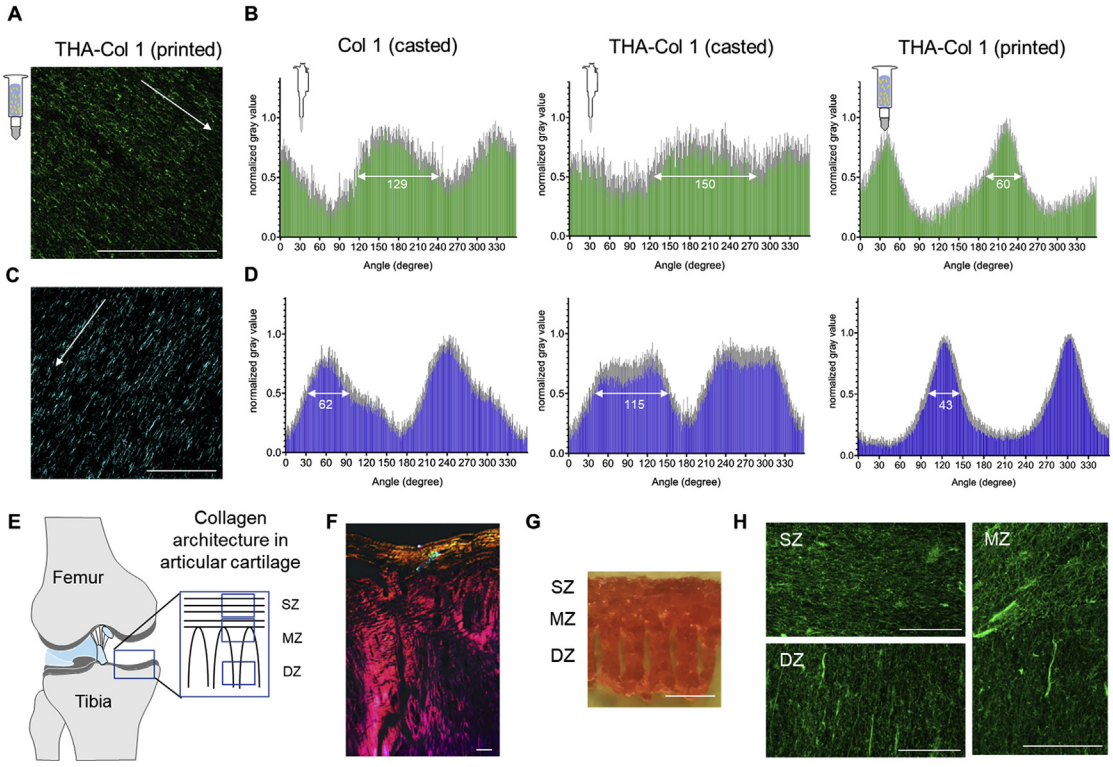

Fig. 5. Three-dimensional printing as a tool to align Col 1 fibers and produce microscopically anisotropic scaffolds. (A) Confocal microscopy of immunofluorescent staining against Col 1 and (C) SHG images demonstrate anisotropic fibers in the THA-Col 1 biomaterial ink (scale bar = 100 μm). Unidirectional orientation of parallel Col 1 fibers aligning along the printing direction (white arrow indicated printing direction). (B and D) Bar diagrams (mean values ± standard deviation) display the quantification of fiber alignment in casted Col 1, casted THA-Col 1 (ID = 1.0 mm), and printed THA-Col 1 (15G: ID = 1.36 mm, 0.25″ cylindrical needle) from images acquired either using the confocal microscope (B, green) or SHG (D, blue). Independent of the microscopical method, the printed THA-Col 1 samples resulted in unidirectional orientation, which was more random for casted THA-Col 1 and Col 1. The white arrow in the bar diagram indicates the peak width at a normalized gray value of 0.5. (E) Schematic illustration of Col 1 fiber alignment in articular cartilage. (F) Polarized light image of articular cartilage illustrating horizontal fibers in the superficial zone (SZ) and vertical orientation in the deep zone (DZ) (scale bar = 50 μm). (G) Macroscopic image of the complex microstructured scaffold (1.4 × 1.6 cm in size, 18G: ID = 0.84 mm, 0.25″ cylindrical needle) mimicking collagen fiber orientation present in articular cartilage (scale bar = 500 μm). (H) Confocal images of immunofluorescent-labeled Col 1 mimicking hierarchical fiber orientation in articular cartilage with parallel horizontal fibers in the SZ, more isotropic fibers in the middle zone (MZ), and parallel vertical fibers in the DZ (scale bar = 50 μm). SHG = second-harmonic generation; THA = tyramine derivative of hyaluronan; ID = inner diameter; SZ = superficial zone; MZ = middle zone; DZ = deep zone.

1.4 × 1.6 cm. The resolution of the printed sample, as shown in Fig. 5G, ranges on the millimeter scale given by the inner diameter of the needle. Immunofluorescent staining against Col 1 clearly shows the fibrillar alignment in the three zones, with horizontal fibers in the SZ, vertical alignment in the DZ, and more isotropic appearance in the MZ.

3.5. Effect of 3DP on cell migration in THA-Col 1 bioink

After characterization of the material microstructure and properties, we investigated the response of hMSCs on aligned anisotropic versus isotropic fibers in the THA-Col 1 bioink. The bioink was either printed using a cylindrical needle or extruded from the cartridge without the needle attached and compared with casted samples. Live/dead staining of hMSC aggregates embedded in THA-Col 1 (printed versus casted) is shown in Fig. 6A at day 1 and 6. The cells were viable after printing and remained viable over culture time. At day 1, some dead cells (stained in red) were visible mainly in the center of the micropellets. After 6 days, the number of dead cells were less than that observed on day 1 in all three groups. The live/dead staining also showed no toxic effect with the addition of H_2O_2 (0.39 mM) in THA and THA-Col 1 to initiate enzymatic gelation.

During *in vitro* culture, hMSCs migrated from the micropellets in all three groups. Observing the cytoskeleton orientation via phalloidin staining, MSC alignment was more pronounced in the printed groups, while hMSCs showed a more isotropic cytoskeletal orientation in the extruded and casted group. The overlay image of actin filament staining (red) and cell nuclei (blue) demonstrated the unidirectional migration of the cells (Fig. 6B).

Fig. 6C illustrates the orientation of the cytoskeleton based on the MAX projection of the red channel. The group printed using a 15G needle (left) displays two clear maxima along the orientation of the Col fibers determined by the printing direction (and at an angle of 180° from it), indicated by the green arrows, thus indicating cytoskeleton alignment along the Col fibers. For the group undergoing extrusion without the needle (2.4-mm diameter, center), the peaks were markedly broadened and more jagged, indicative of a more random distribution; this trend was even more apparent for the casted sample, in which the distribution assumes a white noise profile.

4. Discussion

Extrusion-based printing has achieved significant advances in controlling construct resolution, composition, and shape. However, control over the microscopic architecture has been mostly overlooked. Mechanical and biological properties of animal tissues depend not only on the chemical composition but also on the specific spatial arrangement of structural molecules and biological factors [9]. For example, cartilage is composed of a GAG-based matrix containing Col 1 fibers with specific orientation, parallel to the surface in the SZ and perpendicular in deeper layers [44].

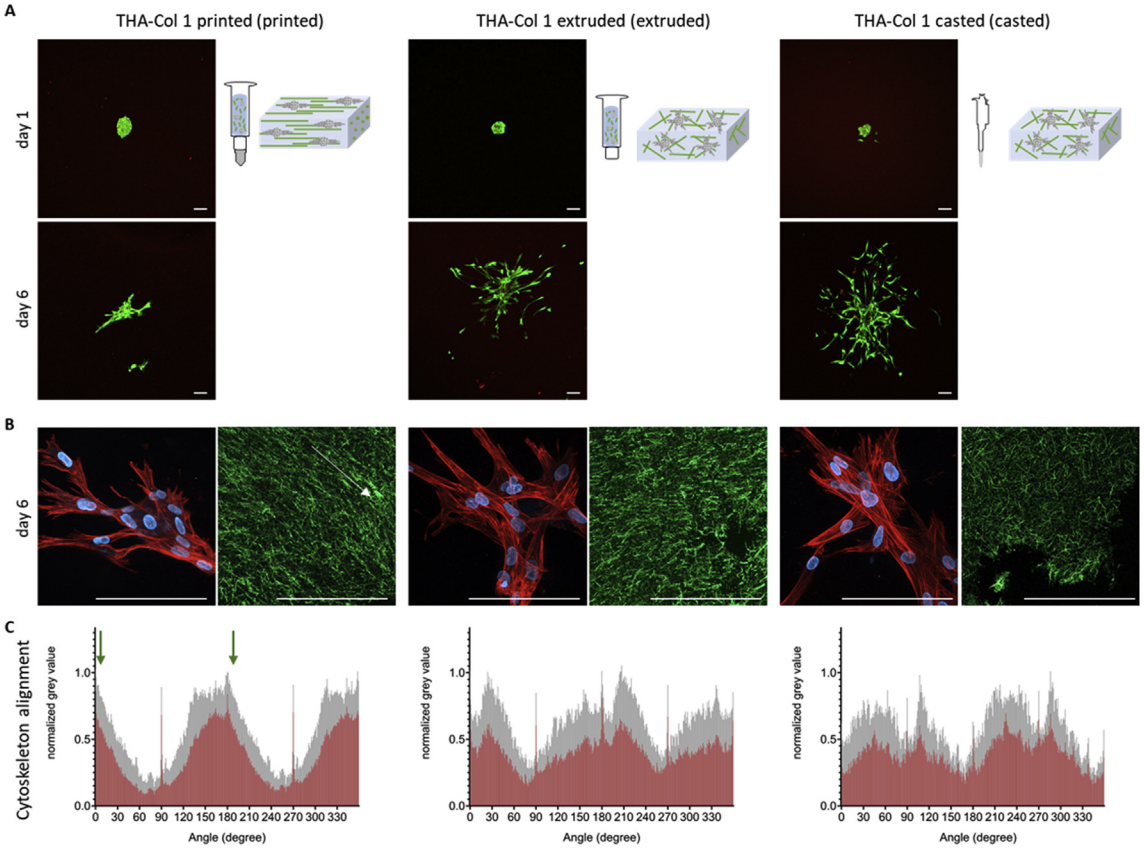

Fig. 6. Viability (live/dead staining) and phalloidin staining of hMSC micropellets in THA-Col 1 hydrogel. (A) Representative images of live/dead staining at day 1 and day 6 showing living cells stained in green with few dead cells stained in red (scale bar = 100 μm). Bioink was either printed using the 15G (ID = 1.36 mm) cylindrical needle, extruded from the 3CC cartridge (ID = 2.4 mm) or pipetted using the CP100-positive displacement pipette (ID = 1.0 mm). (B) MAX z-projection of hMSCs after 6 days of culture in THA-Col 1, demonstrating unidirectional actin filaments/cell cytoskeleton (stained in red) along the Col 1 (stained in green) direction of printed samples (the white arrow indicates printing direction) and cell nuclei (blue). In extruded and casted samples, the cells migrated randomly in the bioink (scale bar = 100 μm). (C) Orientation of the cytoskeleton of hMSCs embedded in THA-Col 1 printed, extruded and casted, displaying the mean values in red with standard deviation in gray. More unidirectional alignment with smaller peak width of the cytoskeleton resulted for 15G-printed THA-Col 1 compared with the two other groups. The green arrow in the graph of printed sample indicates the printing direction. hMSC = human bone marrow–derived mesenchymal stromal cell; THA = tyramine derivative of hyaluronan; ID = inner diameter.

In the present work, we propose a technique to introduce anisotropic properties into a THA-Col 1 composite biomaterial. Having two parallel occurring cross-linking mechanisms, we overcame the difficulty in homogenous mixing of Col 1 fibrils into a viscoelastic HA-based matrix by combining a previously developed bioink based on THA [45] with acidic solubilized Col 1, which was buffered upon mixing, thereby forming fibrils. Because both precursors, THA bioink and Col 1 are in liquid form, mixing to homogeneity was easily achieved, as visualized with microscopic techniques (Fig. 2A–D). A distinctive advantage of the preparation method illustrated here is that THA cross-linking and Col 1 fibril formation occur simultaneously, thus avoiding phase separation [22]. Although the Col 1 fibrils in the confocal and SHG images in Fig. 2 seem to differ between pure Col 1 and THA-Col 1, both casted, there is no difference in fiber diameter as shown by secondary electron and transmission electron microscopy [46]. The visual differences can be explained by the MAX projection of several focus planes within the 3D constructs, and thus, fibers in the deeper regions tend to display smaller fibrils than the fibrils captured in z-directions closer to the objective.

The preservation of the fibrillar microstructure of low concentrated neutral Col 1 (final concentration of 2.5 mg/ml in the composite) within THA (final concentration of 12.5 mg/ml) after 3DP is an additional feature required to produce the anisotropic microstructure.

Casted Col 1 hydrogels have been extensively used in the literature, but the fibrillar structure was not extensively investigated when combined with a second polymer. Binner et al. [47] characterized a star--shaped poly(ethylene glycol) hydrogel mixed with fluorescein isothiocyanate–labeled Col 1. Besides a homogenous distribution of Col 1, no fibrillar structure was shown and further characterized [47]. Formation of Col 1 fibers was found to be dependent on the incubation time at 4 °C before pH neutralization, thus inducing fibrillation when combined with Matrigel [48]. A thermally controlled printing of Col 1 (6 mg/ml) blended with Pluronic (60% w/v) resulted in Col 1 fiber formation and aggregation with a dependency of the fiber alignment on the amount of media added and thus time to dissolve the Pluronic out of the blend [20].

The shear thinning and viscosity behavior of high-concentration neutralized Col 1 (20–60 mg/ml) has been characterized by different groups [19,49]. In contrast, 3DP of neutralized pure Col 1 at low concentrations is challenging owing to the lack of shear thinning and shape retention. At the low concentration used in this study ($\leq$5 mg/ml), printability was rescued by the shear thinning component, THA. A similar approach was presented by Duarte Campos et al. [50] using agarose as the shear thinning component. On the other hand, printing properties of THA previously investigated in our group were preserved upon mixing with Col 1 [51].

The addition of Col 1 to THA increased the storage modulus. Thus, the fibrillar network within the viscoelastic THA can be used as a design parameter to modulate the mechanical properties. The formation of dityramine bonds between Col 1 and THA could be one reason for the synergistic effect [46,52]. Other advantages of the composite are that the cell-mediated shrinking of Col 1 scaffolds is reduced; on the other side, Col 1 provides cell attachment sites to HA and an ECM-mimetic fibrillar matrix. Reduced shrinkage of Col 1 was also observed when this natural material was combined with silk when pulmonary fibroblasts were embedded [52].

Within the casted gels, the fibrils exhibited either random orientation or local domains with some degree of orientation, which could be attributed to the low but non-zero shear forces experienced during casting from a pipette.

After 3DP of the composite, an overall alignment along the printing axis was observed as expected. Therefore, the low-grade enzymatic cross-linking of the THA preserved at least in part the capability of the fibrils to comply with the shear stimulus when extruded.

Not only shear-induced alignment of fibrils but also molecules have been reported in the literature [21,53–56]. Kim et al. [53] controlled the fiber alignment in dependence of the needle diameter during printing, showing a higher degree of alignment when using 30G than when using 20G needles. This intuitive behavior was not observed in the present study; rather, with thinner needles, the fibrillar structure was disrupted, possibly owing to the significantly higher pressure that was needed to achieve extrusion, potentially creating discontinuity or turbulence (supplementary Fig. A1). Moncal et al. [20] introduced Col printing (6 mg/ml) with a thermally controlled setup using Pluronic as the sacrificial material and quantified the alignment of Col fibers along the printing direction related to the amount of media and incubation time (0–48 h) to induce fibrillation but with overall low anisotropy indices. An agarose-Col (5 mg/ml of agarose and 2 mg/ml of Col 1) blend with equally distributed Col fibers but no signs of alignment after printing was presented by Kopf et al. [57]. A different approach to align Col 1 fibers was shown by Betsch et al [58]. They aligned iron nanoparticle–loaded agarose-Col 1 biomaterial ink after exposure to a magnetic field. The alignment was most prevalent in Col 1 (3 mg/ml) compared with the composite (3 mg/ml of agarose, 2.5 mg/ml of Col 1) only in the group with magnetic field exposure [58]. Yang et al. [59] also used electrically assisted printing to mimic Col 1 orientation in the meniscus by radial and circumferential aligned carbon nanotubes. With the method presented here, we achieved alignment of Col 1 fibrils within a composite using exclusively natural ECM molecules avoiding using synthetic non-degradable components simply by 3D extrusion printing. Col 1 only can evolve over time becoming isotropic. This behavior is prevented within the composite owing to the presence of gelled THA stabilizing Col 1 fibrils.

Owing to the signs of Col fibril disruption at high shear stresses indicated by less alignment (Suppplementary Fig. A2) and the decrease in the storage modulus shown with amplitude sweep (Fig. 2G), the resolution of the biomaterial ink introduced here is limited. As shown in Fig. A4, the THA-Col 1 filaments tend to spread owing to their soft properties after enzymatic cross-linking but still allow creation of multilayered crisscross structures at moderate resolution (Supplementary Fig. A4). The more oval shape instead of the rectangular one of the transversal pore geometry within this printed crisscross structure indicates filament fusion to some extent, which was described by Ouyang et al. [60] as one indicator of shape fidelity. Although the resolution of the biomaterial ink is lower than what can be reached in the field, this had no negative effect on the printing of the construct mimicking the fiber orientation of articular cartilage.

The combination of the two ECM components brings biological features and directs cellular behavior. Single-cell seeding resulted in enhanced adhesion, overcoming limited cell attachment reported before [51]. Similar results were observed with cell aggregates, in which the presence of Col 1 increased the migration length and area. This behavior can be attributed to the presence of the integrin interaction site arginine, glycine, and aspartate (RGD sequence) naturally contained in Col 1 inducing cell adhesion [24]. A direct correlation of cell adhesion and RGD density was shown also for electrospun HA functionalized with the RGD peptide by Kim et al. [61]. The agarose-Col blend cited previously has been shown to enhance smooth muscle cell spreading and attachment, thus confirming that the presence of Col 1 in a composite influences cell spreading [57].

Not only the local microstructure of the material but also fiber parameters regulate cell response [62,63]. In this study, hMSC migration was stimulated along the unidirectional orientation of the Col 1 fibers after 3DP. Owing to the interaction of hMSCs with Col 1 fibers, the original orientation of the parallel fiber alignment was less visible in confocal microscopy (Fig. 6B). However, the overlapping direction of cytoskeleton orientation and fiber alignment were visualized and quantified (supplementary Fig. A2). In a comparable study, Kim et al. [53] showed the unidirectional actin filament orientation of keratinocytes embedded in corneal stroma–derived decellularized ECM after printing, which were less pronounced in non-printed samples for preparation of corneal implants. Yang et al. [64] reported an increase in tendon-associated genes of rat MSCs with the oriented Col 1 fiber membrane

compared with the isotropic sample. Whether this observation relies on the anisotropic properties or is partially induced by the shear stress during printing is not fully understood.

HA has been shown to have a plethora of biological properties, including inducing cell proliferation, chondrogenic differentiation, and matrix synthesis [65,66]. The THA-Col 1 composite proposed here supported the migration and chondrogenic differentiation of hMSC micropellets, resulting in cartilage-like matrix deposition throughout the hydrogel. Matrix deposition of hMSCs embedded in THA-Col 1 was uniform, with staining comparable with the standard pellet culture control (Fig. 4E–F). Importantly, despite the presence of Col 1 and invasion of the whole matrix, cell morphology was also comparable with the pellet culture, showing a more condensed rather than spindle-shaped morphology, indicating cell differentiation along chondrogenic lineage. Cells within micropellets are in their preferred 3D condensed environment with high intercellular contact compared with single-cell embedding at high cell density (10–20 Mio/ml) required for *in vitro* chondrogenic differentiation within biomaterials and thus can explain their good prochondrogenic differentiation within the biomaterial. hMSC migration out of micropellets embedded in Col hydrogel subjected to *in vitro* chondrogenic differentiation was also reported by Wang et al. [67] showing that those cells were positively stained for chondrogenic differentiation markers including Col 1 and 2, aggrecan, and SOX9. Good chondrogenic differentiation starting from micropellets or cell aggregates was also reported by Markway et al. [69], whereas Rogan et al [68] observed less chondrogenic differentiation compared with the gold standard in the pellet culture [67]. The biomaterial used in this study overcomes the limitation of ECM deposition only in the pericellular region, which is attributed to many seminatural materials used for cartilage tissue engineering.

One possible concern regarding cartilage regeneration is the use of Col type 1 instead of type 2 for our bioink. Clinical studies of a cell-free type 1 Col hydrogel (CaReS-1S®; Arthro Kinetics AG) implanted in focal, full-layer cartilage defects have shown good clinical outcomes addressing defect filling and the homogenous structure of the repair tissue [28], with Col 1 disappearing *in vivo* to leave space to the cell-deposited Col 2 [30]. In a minipig study, colonization of the cell-free Col 1 matrix gave outcomes comparable with matrix-assisted chondrocyte implantation [25,29]. Jiang et al. [70] demonstrated superior chondrogenic differentiation of MSC embedded in Col 1 compared with MSCs only in a rat model. On the other hand, HA has been combined with Col 1 or gelatin before, with similar outcomes that chondrogenic differentiation is promoted in the composite compared with HA or Col 1 only [71–73].

One limitation of the present technique is the shear-induced alignment, limiting the degrees of spatial freedom in fibril arrangement. Another limitation is the missing quantification of the Col 1 fibers within the composite compared with Col 1 hydrogel and how the microstructural alignment affects cell alignment. This was partially due to technical limitations in visualizing Col 1 fibrils crossing different focus planes within a 3D hydrogel and thus dealing with autofluorescence, light scattering, and the opaque characteristic of the hydrogel. For further development, the capacity of regenerating cartilage or other tissues should be tested by interrogating specifically the effect of the orientation separately from the composition and comparing random oriented or non-fibrillar constructs with aligned constructs.

5. Conclusions

Overall, in this work, we have presented a method to obtain a THA-Col 1 composite with macroscopic homogeneity and microscopic heterogeneity mimicking the macromolecular architecture of native tissues. We achieved a uniform distribution of Col 1 fibers within an HA-based viscoelastic matrix starting from liquid precursors with simultaneous Col 1 fibrillation and HA cross-linking. The orientation of the Col 1 fibers in the 3D printed construct was controlled with shear stress during printing and had a direct impact on cell behavior. The biomaterial ink introduced here can be extended to other fibrillar proteins to produce similar microstructural features. The possibility of printing ECM components with control over microscopic alignment brings biofabrication one step closer to capturing the complexity of biological tissues.

Author contribution

Andrea Schwab: Conceptualization, Methodology, Software, Validation, Formal analysis, Investigation, Data Curation, Writing-Original Draft, Reviewing and Editing. **Christophe Hélary**: Conceptualization, Review and Editing. **Geoff Richards**: Review and Editing, Funding acquisition. **Mauro Alini**: Conceptualization, Review and Editing, Funding acquisition. **David Eglin**: Review and Editing, Project administration, Funding acquisition. **Matteo D'Este**: Conceptualization, Writing-Review and Editing, Supervision, Project administration, Funding acquisition.

Data availability

The processed data required to reproduce these findings are available to download from Mendeley-Data link https://doi.org/10.17632/vcxdk7s8jy.1.

Declaration of competing interest

The authors declare that they have no known competing financial interests or personal relationships that could have appeared to influence the work reported in this paper.

Acknowledgments

This work is part of the osteochondral defect collaborative research program supported by the AO Foundation. This project has been partially supported by “L'Agence Nationale de la Recherche” (ANR) and the Swiss National Science Foundation (SNSF): INDEED project, SNSF's grant number 310030E_189310 and ANR's grant number ANR-19-CE06-0028. The authors acknowledge support of the Scientific Center for Optical and Electron Microscopy ScopeM of the Swiss Federal Institute of Technology ETHZ for acquiring SHG images. The Graubünden Innovationsstiftung is acknowledged for its financial support. The authors thank Dr. Christoph Sprecher for his support with confocal microscopy settings and Luca Ambrosio, MD, for his support setting up the turbidity measurement.

Appendix A. Supplementary data

Supplementary data to this article can be found online at https://doi.org/10.1016/j.mtbio.2020.100058.

References

[1] S.V. Murphy, A. Atala, 3D bioprinting of tissues and organs, Nat. Biotechnol. 32 (8) (2014) 773–785.
[2] M. Hospodiuk, M. Dey, D. Sosnoski, I.T. Ozbolat, The bioink: a comprehensive review on bioprintable materials, Biotechnol. Adv. 35 (2) (2017) 217–239.
[3] F.P.W. Melchels, W.J.A. Dhert, D.W. Hutmacher, J. Malda, Development and characterisation of a new bioink for additive tissue manufacturing, J. Mater. Chem. B 2 (16) (2014) 2282.
[4] J. Malda, J. Visser, F.P. Melchels, T. Jungst, W.E. Hennink, W.J. Dhert, J. Groll, D.W. Hutmacher, 25th anniversary article: engineering hydrogels for biofabrication, Adv. Mater. 25 (36) (2013) 5011–5028.
[5] S.M. Bittner, B.T. Smith, L. Diaz-Gomez, C.D. Hudgins, A.J. Melchiorri, D.W. Scott, J.P. Fisher, A.G. Mikos, Fabrication and mechanical characterization of 3D printed vertical uniform and gradient scaffolds for bone and osteochondral tissue engineering, Acta Biomater. 90 (2019) 37–48.

[6] T.J. Klein, S.C. Rizzi, J.C. Reichert, N. Georgi, J. Malda, W. Schuurman, R.W. Crawford, D.W. Hutmacher, Strategies for zonal cartilage repair using hydrogels, Macromol. Biosci. 9 (11) (2009) 1049–1058.

[7] L.H. Nguyen, A.K. Kudva, N.S. Saxena, K. Roy, Engineering articular cartilage with spatially-varying matrix composition and mechanical properties from a single stem cell population using a multi-layered hydrogel, Biomaterials 32 (29) (2011) 6946–6952.

[8] M.A. Heinrich, W. Liu, A. Jimenez, J. Yang, A. Akpek, X. Liu, Q. Pi, X. Mu, N. Hu, R.M. Schiffelers, J. Prakash, J. Xie, Y.S. Zhang, 3D bioprinting: from benches to translational applications, Small 15 (23) (2019), e1805510.

[9] P. Datta, V. Vyas, S. Dhara, A.R. Chowdhury, A. Barui, Anisotropy properties of tissues: a basis for fabrication of biomimetic anisotropic scaffolds for tissue engineering, JBE 16 (5) (2019) 842–868.

[10] M.D. Shoulders, R.T. Raines, Collagen structure and stability, Annu. Rev. Biochem. 78 (2009) 929–958.

[11] A. Malandrino, X. Trepat, R.D. Kamm, M. Mak, Dynamic filopodial forces induce accumulation, damage, and plastic remodeling of 3D extracellular matrices, PLoS Comput. Biol. 15 (4) (2019), e1006684.

[12] A.D. Doyle, K.M. Yamada, Mechanosensing via cell-matrix adhesions in 3D microenvironments, Exp. Cell Res. 343 (1) (2016) 60–66.

[13] W.M. Han, S.J. Heo, T.P. Driscoll, J.F. Delucca, C.M. McLeod, L.J. Smith, R.L. Duncan, R.L. Mauck, D.M. Elliott, Microstructural heterogeneity directs micromechanics and mechanobiology in native and engineered fibrocartilage, Nat. Mater. 15 (4) (2016) 477–484.

[14] B. Patel, Z. Xu, C.B. Pinnock, L.S. Kabbani, M.T. Lam, Self-assembled collagen-fibrin hydrogel reinforces tissue engineered adventitia vessels seeded with human fibroblasts, Sci. Rep. 8 (1) (2018) 3294.

[15] A.S. Gladman, E.A. Matsumoto, R.G. Nuzzo, L. Mahadevan, J.A. Lewis, Biomimetic 4D printing, Nat. Mater. 15 (4) (2016) 413–418.

[16] S.A. Bradner, M. McGill, A. Golding, R. Grudt, D.L. Kaplan, Silk hydrogel microfibers for biomimetic fibrous material design, Macromol. Mater. Eng. 304 (7) (2019) 1900045.

[17] A. Lode, M. Meyer, S. Bruggemeier, B. Paul, H. Baltzer, M. Schropfer, C. Winkelmann, F. Sonntag, M. Gelinsky, Additive manufacturing of collagen scaffolds by three-dimensional plotting of highly viscous dispersions, Biofabrication 8 (1) (2016), 015015.

[18] N. Diamantides, C. Dugopolski, E. Blahut, S. Kennedy, L.J. Bonassar, High density cell seeding affects the rheology and printability of collagen bioinks, Biofabrication 11 (4) (2019), 045016.

[19] E.O. Osidak, P.A. Karalkin, M.S. Osidak, V.A. Parfenov, D.E. Sivogrivov, F. Pereira, A.A. Gryadunova, E.V. Koudan, Y.D. Khesuani, C.V.A. capital Ka, S.I. Belousov, S.V. Krasheninnikov, T.E. Grigoriev, S.N. Chvalun, E.A. Bulanova, V.A. Mironov, S.P. Domogatsky, Viscoll collagen solution as a novel bioink for direct 3D bioprinting, J. Mater. Sci. Mater. Med. 30 (3) (2019) 31.

[20] K.K. Moncal, V. Ozbolat, P. Datta, D.N. Heo, I.T. Ozbolat, Thermally-controlled extrusion-based bioprinting of collagen, J. Mater. Sci. Mater. Med. 30 (5) (2019) 55.

[21] B.A. Nerger, P.T. Brun, C.M. Nelson, Microextrusion printing cell-laden networks of type I collagen with patterned fiber alignment and geometry, Soft Matter 15 (28) (2019) 5728–5738.

[22] S. Rhee, J.L. Puetzer, B.N. Mason, C.A. Reinhart-King, L.J. Bonassar, 3D bioprinting of spatially heterogeneous collagen constructs for cartilage tissue engineering, ACS Biomater. Sci. Eng. 2 (10) (2016) 1800–1805.

[23] R.V. Iozzo, L. Schaefer, Proteoglycan form and function: a comprehensive nomenclature of proteoglycans, Matrix Biol. 42 (2015) 11–55.

[24] M. Baniasadi, M. Minary-Jolandan, Alginate-collagen fibril composite hydrogel, Materials (Basel) 8 (2) (2015) 799–814.

[25] K. Gavenis, U. Schneider, U. Maus, T. Mumme, R. Muller-Rath, B. Schmidt-Rohlfing, S. Andereya, Cell-free repair of small cartilage defects in the Goettinger minipig: which defect size is possible? Knee Surg. Sports Traumatol. Arthrosc. 20 (11) (2012) 2307–2314.

[26] C.D. Reyes, A.J. García, Engineering integrin-specific surfaces with a triple-helical collagen-mimetic peptide, J. Biomed. Mater. Res. 65A (4) (2003) 511–523.

[27] S. Andereya, U. Maus, K. Gavenis, R. Muller-Rath, O. Miltner, T. Mumme, U. Schneider, [First clinical experiences with a novel 3D-collagen gel (CaReS) for the treatment of focal cartilage defects in the knee], Z. Orthop. Ihre Grenzgeb. 144 (3) (2006) 272–280.

[28] T. Efe, C. Theisen, S. Fuchs-Winkelmann, T. Stein, A. Getgood, M.B. Rominger, J.R. Paletta, M.D. Schofer, Cell-free collagen type I matrix for repair of cartilage defects-clinical and magnetic resonance imaging results, Knee Surg. Sports Traumatol. Arthrosc. 20 (10) (2012) 1915–1922.

[29] U. Schneider, B. Schmidt-Rohlfing, K. Gavenis, U. Maus, R. Mueller-Rath, S. Andereya, A comparative study of 3 different cartilage repair techniques, Knee Surg. Sports Traumatol. Arthrosc. 19 (12) (2011) 2145–2152.

[30] K.F. Schuettler, J. Struewer, M.B. Rominger, P. Rexin, T. Efe, Repair of a chondral defect using a cell free scaffold in a young patient–a case report of successful scaffold transformation and colonisation, BMC Surg. 13 (2013) 11.

[31] J. Zhu, L.J. Kaufman, Collagen I self-assembly: revealing the developing structures that generate turbidity, Biophys. J. 106 (8) (2014) 1822–1831.

[32] S. Zhu, Q. Yuan, T. Yin, J. You, Z. Gu, S. Xiong, Y. Hu, Self-assembly of collagen-based biomaterials: preparation, characterizations and biomedical applications, J. Mater. Chem. B 6 (18) (2018) 2650–2676.

[33] N. Latifi, M. Asgari, H. Vali, L. Mongeau, A tissue-mimetic nano-fibrillar hybrid injectable hydrogel for potential soft tissue engineering applications, Sci. Rep. 8 (1) (2018) 1047.

[34] C. Loebel, M. D'Este, M. Alini, M. Zenobi-Wong, D. Eglin, Precise tailoring of tyramine-based hyaluronan hydrogel properties using DMTMM conjugation, Carbohydr. Polym. 115 (2015) 325–333.

[35] B. Hoyer, A. Bernhardt, A. Lode, S. Heinemann, J. Sewing, M. Klinger, H. Notbohm, M. Gelinsky, Jellyfish collagen scaffolds for cartilage tissue engineering, Acta Biomater. 10 (2) (2014) 883–892.

[36] M.S. Saravanan, J. Jayamani, G. Shanmugam, B. Madhan, High concentration of propanol does not significantly alter the triple helical structure of type I collagen, Colloid Polym. Sci. 293 (9) (2015) 2655–2662.

[37] K. Kar, P. Amin, M.A. Bryan, A.V. Persikov, A. Mohs, Y.H. Wang, B. Brodsky, Self-association of collagen triple helic peptides into higher order structures, J. Biol. Chem. 281 (44) (2006) 33283–33290.

[38] B.R. Williams, R.A. Gelman, D.C. Poppke, K.A. Piez, Collagen fibril formation. Optimal in vitro conditions and preliminary kinetic results, J. Biol. Chem. 253 (18) (1978) 6578–6585.

[39] O.F. Gardner, M. Alini, M.J. Stoddart, Mesenchymal stem cells derived from human bone marrow, Methods Mol. Biol. 1340 (2015) 41–52.

[40] C. Loebel, T. Stauber, M. D'Este, M. Alini, M. Zenobi-Wong, D. Eglin, Fabrication of cell-compatible hyaluronan hydrogels with a wide range of biophysical properties through high tyramine functionalization, J. Mater. Chem. B 5 (12) (2017) 2355–2363.

[41] R. Tognato, A.R. Armiento, V. Bonfrate, R. Levato, J. Malda, M. Alini, D. Eglin, G. Giancane, T. Serra, A stimuli-responsive nanocomposite for 3D anisotropic cell-guidance and magnetic soft robotics, Adv. Funct. Mater. 29 (9) (2019) 1804647.

[42] C.E. Ayres, B.S. Jha, H. Meredith, J.R. Bowman, G.L. Bowlin, S.C. Henderson, D.G. Simpson, Measuring fiber alignment in electrospun scaffolds: a user's guide to the 2D fast Fourier transform approach, J. Biomater. Sci. Polym. Ed. 19 (5) (2008) 603–621.

[43] R. Farndale, D. Buttle, A. Barrett, Improved quantitation and discrimination of sulphated glycosaminoglycans by use of dimethylmethylene blue, Biochim. Biophys. Acta Gen. Subj. 883 (2) (1986) 173–177.

[44] J.A. Buckwalter, V.C. Mow, A. Ratcliffe, Restoration of injured or degenerated articular cartilage, J. Am. Acad. Orthop. Surg. 2 (4) (1994) 192–201.

[45] D. Petta, A.R. Armiento, D. Grijpma, M. Alini, D. Eglin, M. D'Este, 3D bioprinting of a hyaluronan bioink through enzymatic-and visible light-crosslinking, Biofabrication 10 (4) (2018), 044104.

[46] A. Frayssinet, D. Petta, C. Illoul, B. Haye, A. Markitantova, D. Eglin, G. Mosser, M. D'Este, C. Helary, Extracellular matrix-mimetic composite hydrogels of cross-linked hyaluronan and fibrillar collagen with tunable properties and ultrastructure, Carbohydr. Polym. 236 (2020) 116042.

[47] M. Binner, L.J. Bray, J. Friedrichs, U. Freudenberg, M.V. Tsurkan, C. Werner, Cell-instructive starPEG-heparin-collagen composite matrices, Acta Biomater. 53 (2017) 70–80.

[48] K.V. Nguyen-Ngoc, A.J. Ewald, Mammary ductal elongation and myoepithelial migration are regulated by the composition of the extracellular matrix, J. Microsc. 251 (3) (2013) 212–223.

[49] A.D. Nocera, R. Comin, N.A. Salvatierra, M.P. Cid, Development of 3D printed fibrillar collagen scaffold for tissue engineering, Biomed. Microdevices 20 (2) (2018) 26.

[50] D.F. Duarte Campos, M. Rohde, M. Ross, P. Anvari, A. Blaeser, M. Vogt, C. Panfil, G.H. Yam, J.S. Mehta, H. Fischer, P. Walter, M. Fuest, Corneal bioprinting utilizing collagen-based bioinks and primary human keratocytes, J. Biomed. Mater. Res. 107 (9) (2019) 1945–1953.

[51] D. Petta, D.W. Grijpma, M. Alini, D. Eglin, M. D'Este, Three-Dimensional printing of a tyramine hyaluronan derivative with double gelation mechanism for independent tuning of shear thinning and postprinting curing, ACS Biomater. Sci. Eng. 4 (8) (2018) 3088–3098.

[52] A. Sundarakrishnan, H. Zukas, J. Coburn, B.T. Bertini, Z. Liu, I. Georgakoudi, L. Baugh, Q. Dasgupta, L.D. Black, D.L. Kaplan, Bioengineered in vitro tissue model of fibroblast activation for modeling pulmonary fibrosis, ACS Biomater. Sci. Eng. 5 (5) (2019) 2417–2429.

[53] H. Kim, J. Jang, J. Park, K.P. Lee, S. Lee, D.M. Lee, K.H. Kim, H.K. Kim, D.W. Cho, Shear-induced alignment of collagen fibrils using 3D cell printing for corneal stroma tissue engineering, Biofabrication 11 (3) (2019), 035017.

[54] J. Lin, Y. Shi, Y. Men, X. Wang, J. Ye, C. Zhang, Mechanical roles in formation of oriented collagen fibers, Tissue Eng. B Rev. 26 (2) (2020) 116–128.

[55] A. Kamada, A. Levin, Z. Toprakcioglu, Y. Shen, V. Lutz-Bueno, K.N. Baumann, P. Mohammadi, M.B. Linder, R. Mezzenga, T.P.J. Knowles, Modulating the mechanical performance of macroscale fibers through shear-induced alignment and assembly of protein nanofibrils, Small 16 (9) (2020) 1904190.

[56] M.K. Hausmann, P.A. Ruhs, G. Siqueira, J. Lauger, R. Libanori, T. Zimmermann, A.R. Studart, Dynamics of cellulose nanocrystal alignment during 3D printing, ACS Nano 12 (7) (2018) 6926–6937.

[57] M. Kopf, D.F. Campos, A. Blaeser, K.S. Sen, H. Fischer, A tailored three-dimensionally printable agarose-collagen blend allows encapsulation, spreading, and attachment of human umbilical artery smooth muscle cells, Biofabrication 8 (2) (2016), 025011.

[58] M. Betsch, C. Cristian, Y.Y. Lin, A. Blaeser, J. Schoneberg, M. Vogt, E.M. Buhl, H. Fischer, D.F. Duarte Campos, Incorporating 4D into bioprinting: real-time magnetically directed collagen fiber alignment for generating complex multilayered tissues, Adv. Healthc. Mater. 7 (21) (2018), e1800894.

[59] Y. Yang, Z. Chen, X. Song, Z. Zhang, J. Zhang, K.K. Shung, Q. Zhou, Y. Chen, Biomimetic anisotropic reinforcement architectures by electrically assisted nanocomposite 3D printing, Adv. Mater. 29 (11) (2017).

[60] L. Ouyang, R. Yao, Y. Zhao, W. Sun, Effect of bioink properties on printability and cell viability for 3D bioplotting of embryonic stem cells, Biofabrication 8 (3) (2016), 035020.
[61] I.L. Kim, S. Khetan, B.M. Baker, C.S. Chen, J.A. Burdick, Fibrous hyaluronic acid hydrogels that direct MSC chondrogenesis through mechanical and adhesive cues, Biomaterials 34 (22) (2013) 5571–5580.
[62] A.D. Doyle, N. Carvajal, A. Jin, K. Matsumoto, K.M. Yamada, Local 3D matrix microenvironment regulates cell migration through spatiotemporal dynamics of contractility-dependent adhesions, Nat. Commun. 6 (2015) 8720.
[63] T.L. Jenkins, D. Little, Synthetic scaffolds for musculoskeletal tissue engineering: cellular responses to fiber parameters, NPJ Regen. Med. 4 (2019) 15.
[64] S. Yang, X. Shi, X. Li, J. Wang, Y. Wang, Y. Luo, Oriented collagen fiber membranes formed through counter-rotating extrusion and their application in tendon regeneration, Biomaterials 207 (2019) 61–75.
[65] R. Mohan, N. Mohan, D. Vaikkath, Hyaluronic acid dictates chondrocyte morphology and migration in composite gels, Tissue Eng. A 24 (19–20) (2018) 1481–1491.
[66] E. Amann, P. Wolff, E. Breel, M. van Griensven, E.R. Balmayor, Hyaluronic acid facilitates chondrogenesis and matrix deposition of human adipose derived mesenchymal stem cells and human chondrocytes co-cultures, Acta Biomater. 52 (2017) 130–144.
[67] Y. Xiao, S. Long, Y. Fan, X. Zhang, Role of N-cadherin in a niche-mimicking microenvironment for chondrogenesis of mesenchymal stem cells in vitro, ACS Biomater. Sci. Eng. 6 (6) (2020) 3491–3501, https://doi.org/10.1021/acsbiomaterials.0c00149.
[68] H. Rogan, F. Ilagan, F. Yang, Comparing single cell versus pellet encapsulation of mesenchymal stem cells in three-dimensional hydrogels for cartilage regeneration, Tissue Eng. A 25 (19–20) (2019) 1404–1412.
[69] B.D. Markway, G.K. Tan, G. Brooke, J.E. Hudson, J.J. Cooper-White, M.R. Doran, Enhanced chondrogenic differentiation of human bone marrow-derived mesenchymal stem cells in low oxygen environment micropellet cultures, Cell Transplant. 19 (1) (2010) 29–42.
[70] X. Jiang, X. Huang, T. Jiang, L. Zheng, J. Zhao, X. Zhang, The role of Sox9 in collagen hydrogel-mediated chondrogenic differentiation of adult mesenchymal stem cells (MSCs), Biomater. Sci. 6 (6) (2018) 1556–1568.
[71] C.G. Pfeifer, A. Berner, M. Koch, W. Krutsch, R. Kujat, P. Angele, M. Nerlich, J. Zellner, Higher ratios of hyaluronic acid enhance chondrogenic differentiation of human MSCs in a hyaluronic acid-gelatin composite scaffold, Materials (Basel) 9 (5) (2016).
[72] V. Moulisova, S. Poveda-Reyes, E. Sanmartin-Masia, L. Quintanilla-Sierra, M. Salmeron-Sanchez, G. Gallego Ferrer, Hybrid protein-glycosaminoglycan hydrogels promote chondrogenic stem cell differentiation, ACS Omega 2 (11) (2017) 7609–7620.
[73] J. Yang, Y. Liu, L. He, Q. Wang, L. Wang, T. Yuan, Y. Xiao, Y. Fan, X. Zhang, Icariin conjugated hyaluronic acid/collagen hydrogel for osteochondral interface restoration, Acta Biomater. 74 (2018) 156–167.